FRACTAL ANALYSIS OF LIQUID ATOMIZATION PROCESSES: PART 2: APPLICATIONS

Sébastien Grout, Jean Cousin, Christophe Dumouchel

Paper ID ICLASS06-051

FRACTAL ANALYSIS OF LIQUID ATOMIZATION PROCESSES. PART 2: APPLICATIONS

Sébastien Grout, Dr. Jean Cousin, Dr. Christophe Dumouchel

CNRS UMR 6614 – CORIA, Université et INSA de Rouen
76801 Saint Etienne du Rouvray, France
email: *name*@coria.fr

ABSTRACT This work, presented in two parts, investigates the relevance of using fractal analysis to characterize and study liquid flow atomization processes. In the first part, it was shown that the EDM methods to determine the fractal dimension was the best adapted to measure either textural or structural local fractal dimension. The part of this study, which is reported in the present paper, shows applications of this analysis on liquid flow issuing from a simplified cavity nozzle. It is first shown that the atomizing liquid flows are fractal and that a fractal analysis is therefore relevant. Second, it is found that the fractal dimension of the flow just at the nozzle exit is textural and that this dimension is related to the issuing liquid flow Reynolds number, i.e., to the turbulent level of the flow. Third, the shape of the liquid flow at the bottom of the atomization process is associated to a structural fractal dimension whose value is related to the liquid gas surface tension.

Keywords: Primary liquid atomization, fractal analysis

1. INTRODUCTION

Among the problems related to the formation of spray from the disintegration of a liquid flow, the primary atomization stage has received little attention so far from an experimental point of view. The primary atomization process designates the stage where drops and ligaments detach from the continuous liquid flow, that is the liquid flow connected to the nozzle. Chigier [1] pointed out that this stage is of paramount importance since it is the vital link between the liquid emerging from the nozzle and the fully developed spray. Furthermore, he emphasized that image analyzing techniques should be developed to study the behavior of atomizing liquid flow because it is the sole technique that allows obtaining information on the liquid break-up.

An atomizing liquid flow is an object with a complex boundary whose area increases due to the growth of perturbations until break-up takes place. The analysis of such objects can be conducted by using fractal dimension concept. An introduction on this concept as well as to the methods available to measure fractal dimensions can be found in [2] and [3], respectively. The use of fractal dimension to analyze atomizing liquid flows has received very little attention so far. The pioneer work in this domain is due to Shavit and Chigier [4] who analyzed the fractal characteristics of a liquid jet atomized by a surrounding high speed gaseous flow. More recently, a similar study was carried out on liquid jets produced at low injection pressure in a gaseous environment at rest [5]. Both approaches provided very encouraging results that suggest to persevere in this direction. However, two important points were not investigated in these approaches. The first one concerns the method to be used to determine the fractal dimension, and the second one concerns the relevance of using the fractal concept to characterize liquid flow. The present study investigates these two points on atomizing liquid flows produced by low injection pressure simplified compound nozzles identical to those studied in recent works [5-6]. The most adapted technique to study such flows has been investigated in a preliminary work [7]. The second point is investigated in the present article following the procedure suggested by Smith et al. [3] in order to know whether a liquid atomization is a fractal or a multi-fractal process. The determination and use of a mean fractal dimension to characterize an atomizing liquid flow is acceptable and meaningful in the first case only.

The 2D liquid flow images that are analyzed in the present work are described in the next section and the application and results of the methodology described in [7] are presented in the third section.

2. ELABORATION OF THE ATOMIZING LIQUID FLOW CONTOURS

2.1 Experimental Conditions

The injection system is a simplified cavity nozzle inspired from compound injectors used in low pressure gasoline injection. The nozzle of the injector used in the present investigation is schematized in Fig. 1. It is constituted of a superposition of three circular disks. The liquid enters the nozzle through disk 1, flows through the cavity disk (disk 2) and discharges through the orifice in disk 3. Disk 1 has a thickness equal to 177 µm and a diameter hole equal to 300 µm. The cavity disk is 75 µm thick and the cavity diameter is equal to 2,254 µm. The discharge orifice disk (disk 3) is characterized by a thickness equal to 76 µm, an orifice hole diameter equal to 180 µm and an eccentricity of 200 µm.

Four liquids are used. They differ by their physical properties that are given in Table 1. Compared to water, Heptane is characterized by smaller surface tension and viscosity and the two mixtures of water/glycerol show a greater viscosity but a similar surface tension. Throughout the study, the injection pressure is kept low and varies from 0.1 to 0.5 MPa.

Table 1: Liquid physical properties.

Liquid	ρ_L (kg/m^3)	μ (kg/m.s)	σ (N/m)	C_D (-)
Water	984	1.00 10^{-3}	0.0720	0.63
Heptane	704	0.41 10^{-3}	0.0206	0.63
Water/Glycerol (5%)	1012	1.33 10^{-3}	0.0704	0.63
Water/Glycerol (10%)	1030	1.43 10^{-3}	0.0702	0.61

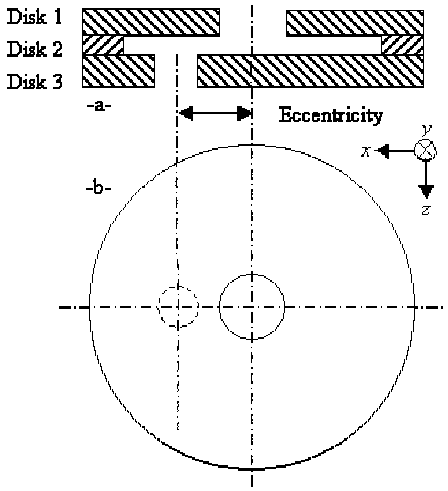

Figure 1: Schematic view of the simplified cavity nozzle: a – Side view. b – Top view.

The behavior of simplified cavity nozzles similar to the one used in the present study was analyzed in a previous investigation [6]. Because the discharge orifice diameter and the injection pressure are small, the Weber number of the issuing liquid is low regardless the liquid (not greater than 7). Such low Weber numbers characterize liquid jets that are not influenced by aerodynamic forces [8]. Thus, the break-up of the liquid flow is mainly controlled by the action of the surface tension forces. Furthermore, because of the nozzle eccentricity and of the small thickness of the cavity disk, the internal liquid flow is subject to drastic deflections that promote the development of a complex structure of the issuing flow. At the exit section, the flow shows a double swirl as well as a consistent turbulent level and it was shown that the atomization efficiency of the nozzle is controlled by the sum of the turbulent and non-axial kinetic energies [6].

For each experimental condition, the volume flow rate is measured by weighting the liquid collected during a controlled time interval and the discharge coefficient C_D is calculated. This coefficient is defined by:

$$C_D = \frac{Q_v}{S\sqrt{\frac{2\Delta P_i}{\rho_L}}} \qquad (1)$$

where Q_v is the volume flow rate, ΔP_i the injection pressure, ρ_L the liquid density and S the area of the discharge orifice. For each liquid, the discharge coefficient is found independent of the injection pressure. The discharge coefficients obtained for each liquid are shown in Table 1. It can be noted that they vary very little from one liquid to another with, as expected, the smallest value for the more viscous liquid.

The visualization of the issuing liquid flow is performed with a Fuji Digital Camera (FinePix SI Pro, Fujifilm, Japan) which offers a high resolution of 3,040x2,016 pixel^2 and a distribution of light intensity on 256 levels for each of the three color frame components (Red, Green, Blue). A Nanotwin Flash System (HSPS) was used to enlighten the liquid flow. This light source produces very short light flashes (≈ 11 ns). The light source, the liquid flow and the camera were aligned in a backlight image configuration. The light intensity was concentrated on the liquid flow by a 140 mm focal length lens. The field of visualization covered a 10.5x7 mm^2 area corresponding to a spatial resolution of 3.5 µm/pixel and the depth of field was equal to 7 mm. According to the discharge coefficient and to the range of injection pressures, the maximum flowing velocity of the issuing liquid flow is of the order of 25 m/s. The corresponding displacement during the flash duration is equal to 0.25 µm. It is far less than the spatial resolution. Thus, the issuing liquid flows are well frozen. For each working conditions (fluid, injection pressure) 150 images are recorded.

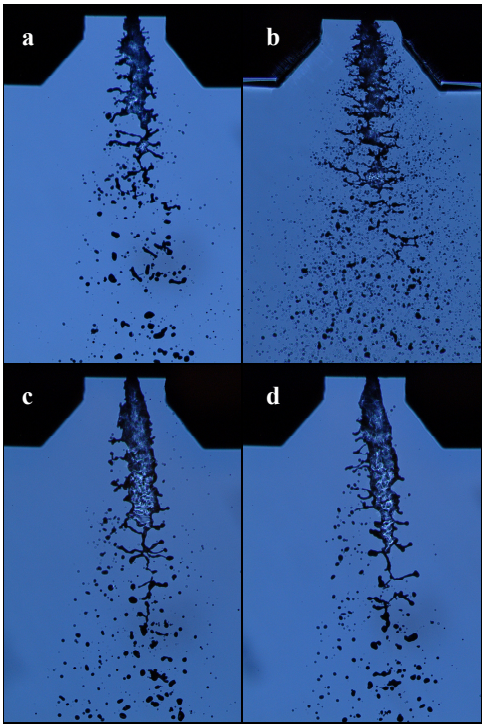

Figure 2: Visualizations in the (O, x, z) plane (ΔP_i = 0.35 MPa) a – Water, b – Heptane, c – Water/Glycerol 5%, d – Water/Glycerol 10%

Example of images obtained at 0.35 MPa and with each fluid are presented in Fig. 2. It can be noted that the liquid flow is well frozen and that the contrast is very good. The

comparison of the four images illustrates the important role of the surface tension forces on the break-up scheme: characteristic break-up length scales clearly decrease as the liquid-air surface tension coefficient decreases. Figure 2 also shows that the flow issuing from the nozzle does not keep the axisymmetry of the discharge orifice but spreads in the (0, x, z) plane (see Fig. 1 for coordinate system): the disintegration process is organized in this plane. Thus, it appeared relevant to analyze the issuing liquid flows in this plane only. This is what is done in the present study.

2.2 Image Analyzing Technique

The fractal analysis is performed on the continuous liquid flow only. Detached droplets and ligaments are not taken into account and are removed from the image. The analyzing technique to detect the continuous flow contour from the images is improved compared to the previous investigation [5]. It is conducted on the blue frame of the images since its 256 level distribution reported the largest dynamics. This distribution shows a main peak corresponding to the background pixel population. The liquid pixel gray level distribution cover the all level dynamics because of light scattering effects. A double threshold technique is applied to dissociate liquid and background pixels. Two thresholds are determined from the gray level distribution main peak position: gray levels between these thresholds represent background pixels and are attributed the level 255 (white), the others represent liquid pixels and are attributed the level 0 (black). The good contrast of the images ensures a limited influence of the thresholds on the liquid-gas interface determination. An example of application of the double threshold technique is shown in Fig. 3. Figure 3a shows the initial image (detail) and Fig. 3b the corresponding two-gray level one. It can be observed that a non negligible amount of liquid pixels have been interpreted as background ones. This is mainly observed at the bottom of the continuous liquid flows where thin liquid lamella can be produced. The presence of these pixels increases the amount of liquid gas interface (see Fig. 3b) and the external boundary of the liquid flow shows additional and pretty tortuous contour (see Fig. 3c). This additional contour could considerably affect the fractal analysis and it was therefore minimized by applying a dilation-erosion step before the contour detection.

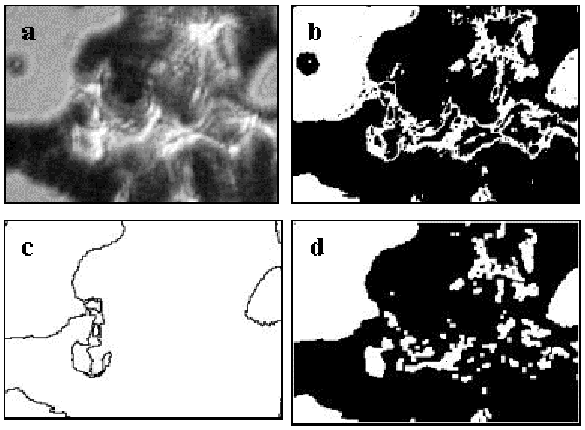

Figure 3: Example of the influence of the dilation-erosion step

The dilation-erosion is a two step procedure. First, a dilation of the object is performed on the two gray level image (Fig. 3b). This step consists in replacing each white pixel with at least one black neighbor by a black pixel. Each gap of one or two pixels wide is filled. Second, an erosion step is applied to compensate the influence of the dilation on the external liquid flow boundary. This step consists in replacing each black pixel with at least one white neighbor by a white one. This does not reopen the small gaps filled during the dilation step. The result of the dilation-erosion step is illustrated in Fig. 3d and shows to which extend the problem of additional external interface creation is limited. Indeed, the application of the detection in Fig. 3d will not penetrate the liquid flow anymore.

The final step of the image analysis is the external contour detection. As recommended by Foroutan-pour et al. [9] fractal analysis should be conducted on skeletal images. This recommendation has been followed in the present analysis.

3. FRACTAL ANALYSIS

All details of the fractal analysis procedure are described in [7] and are not presented in this article. In summary, local fractal analysis is performed on portions of the liquid flow delimited by an analyzing window of 256 pixels height and as wide as the image. The analyzed images show portions of contour and not closed objects. In this condition, the Euclidean Distance Mapping method (EDM) is well adapted and can predict reliable information even when analyzing a single image [7]. An example of the application of the EDM method on one image is presented in Fig. 4. This figure shows the image together with the corresponding contour on which the short dash boxes shows the analyzing window positioned at 200 pixels from the nozzle.

The procedure to determine the fractal characteristics is inspired from Panico and Sterling [10] and makes use of the local slope graph. This graph shows the local slope of the Richardson-Mandelbrot plot as a function of the spatial scale. The EDM method is applied for a spatial scale ranging from 1 to 257 pixels throughout the analysis (see details in [7]). A fractal contour should report a constant local slope over a spatial scale interval. This interval is related to the physical scales over which the shape self similarity is observed. In Fig.4, local slope graphs of the Richardson-Mandelbrot plot are shown for several positions of the analyzing window, ranging from the nozzle exit ($h = 0.7$ mm) to the bottom of the atomization process ($h = 4.55$ mm). For the image analyzed in Fig. 4 the break-up length L_{BU}, that is given by the position of the farthest contour pixel from the nozzle, is equal to 5.18 mm.

Each graph in Fig. 4 shows a spatial scale interval over which the local slope is constant. This interval as well as the corresponding value of the local slope are functions of the distance from the nozzle. Thus, at each position, fractal characteristics of the liquid gas interface can be determined.

Near the nozzle ($h = 0.7$ and 1.4 mm in Fig. 4), constant local slopes are obtained in the medium spatial scale interval, namely, [75 pixel; 125 pixel]. Above this interval, the local slope increases sharply. Referring to the

tests conducted with the EDM method in comparable situations [7], it can be said that the fractal dimension given by the constant local slope characterizes the tortuosity of the liquid gas interface and is referred as the textural fractal dimension [2]. The increase of the local slope above spatial scale of 125 pixel comes from the fact that the method does not analyze the border of the liquid flow anymore but the whole structure of the flow. Thus, the spatial scale at which the local slope increases is related to the width of the liquid flow. It can be noted in Fig. 4 that this spatial scale increases with the downstream position which is due to the enlargement of the liquid flow near the nozzle (see the image in Fig. 4). The results obtained near the nozzle show also that the textural fractal dimension of the liquid flow increases with the downstream distance. This increase indicates a more and more tortuous interface due to the growth of perturbations.

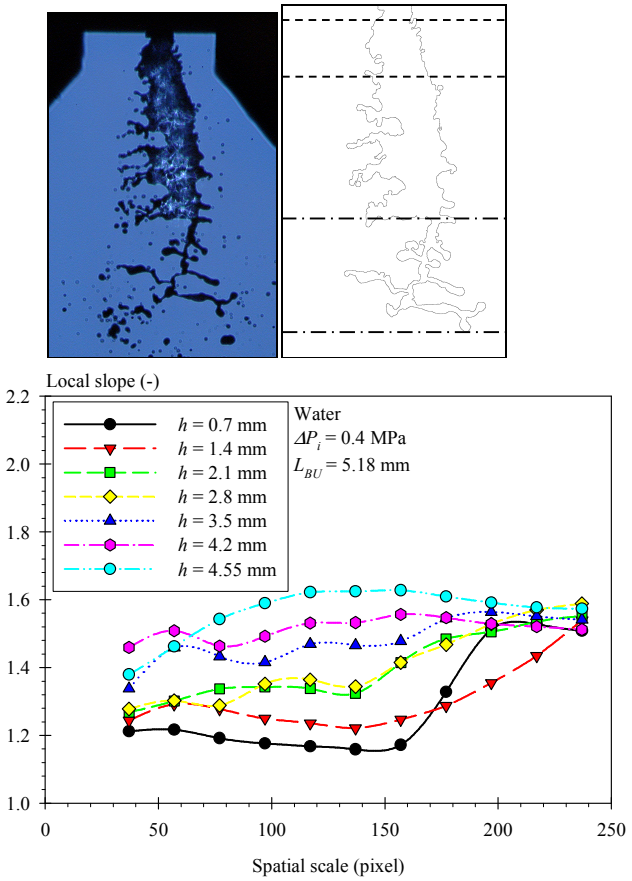

Figure 4: Application of the EDM on one image: Image, contour and local slope graph at several positions in the jet (water, $\Delta P_i = 0.4$ MPa)

Far from the nozzle (h = 4.2 – 4.55 mm), the local slope curves are different. They increase at small spatial scales and reach a constant value above a spatial scale of the order of 110 pixels. At the bottom of the atomization process it can be seen in Fig. 4 that the flow is totally reorganized as a ligament network. Thus, the fractal dimension associated to the constant local slope region characterizes the whole structure of the jet and is referred as the structural fractal dimension [2]. The large spatial scale interval over which the liquid flow is structurally fractal is related to the dispersion of the ligament length and thickness.

For intermediate distances from the nozzle (between 2 and 4 mm), the local slope graphs report zones of increase alternated with two zones of constant value. The constant local slope obtained for the medium spatial interval characterizes the textural fractal dimension of the flow and the one reached for large spatial scale characterizes the structural fractal dimension of the flow.

It can be noted in Fig. 4 that the textural fractal dimension measured near the nozzle is less than the structural fractal dimension characterizing the ligament network far from the nozzle. This indicates that the interface area production rate due to the perturbation growth near the nozzle is less than the one due to the reorganization of the flow at the end of the atomization process. In the present analysis, we will focus on these two fractal characteristics of the flow. The textural fractal dimension near the nozzle is expected to be related to the characteristic of the issuing liquid flow and the structural fractal dimension of the ligament network is expected to be related to the drop size distribution since most of the drops (in term of liquid volume) are likely produced from the break-up of these ligaments.

The results obtained above indicate that the liquid contour analyzed in Fig. 4 shows fractal characteristics that evolve from the nozzle exit to the end of the atomization process. Such a behavior was reported by previous investigations [4, 5]. According to Smith et al. [3] it can be said that the contour representing the continuous liquid flow during the primary atomization process is a multi-fractal object. This characteristic is due to the fact that one contour (as the one analyzed in Fig. 4) shows different stages of the primary atomization process. The initial stage (behavior of the jet at the nozzle exit) is characterized by a textural fractal dimension and a width of the liquid flow. The final stage (behavior of the liquid ligament network) is characterized by a structural fractal dimension. This observation somehow validates the local analysis performed in the present work and suggests that the determination of global fractal dimension would be less meaningful.

An interesting question to be addressed at this point of the analysis is whether each primary atomization stage is a fractal process? To answer this question, the distribution of the fractal dimension for each atomization stage should be studied. According to Smith et al. [3], uniform fractal process would report a distribution that extend on a quite small range of fractal dimension. In the present analysis, fractal dimension distribution can be constructed on the basis of the results reported by the application of the EDM method on series of 150 images available for each working condition. Fractal dimension distributions are examined for the textural fractal dimension of the initial stage and for the structural fractal dimension of the final stage (liquid ligament network).

Figure 5 shows the distribution of the textural fractal dimension measured just at the nozzle exit (h = 0.7 mm). The construction of this distribution makes use of the results given in Fig. 4 where the local slope is found constant within the spatial range [75 pixels; 125 pixels] for

the first position of the analyzing window. The EDM method is thus applied on the 150 available images and the fractal dimension is deduced on the individual Richardson-Mandelbrot plot from the local slope calculated on the [75 pixels; 125 pixels] interval.

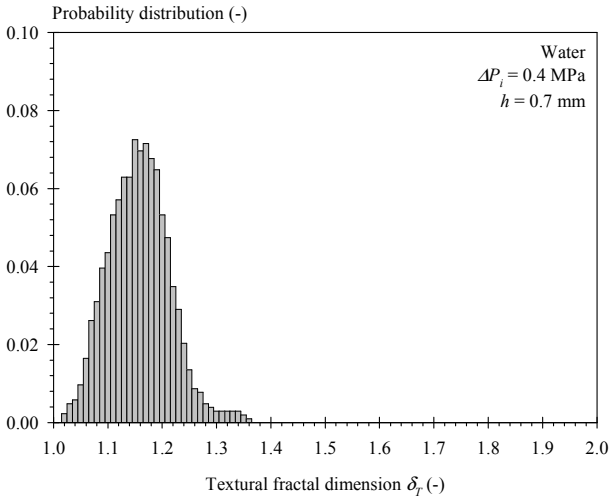

Figure 5: Distribution of the textural fractal dimension near the nozzle (initial atomization stage). (Water, ΔP_i = 0.4 MPa, h = 0.7 mm)

The distribution obtained in Fig. 5 shows a nice bell shape with a clear maximum. The width of this distribution is not as small as it can be obtained for uniform (or linear) fractal objects as shown by Smith et al. [3]. However, we must consider the fact that, although the application of the EDM method on one image is possible, the result obtained might be slightly inaccurate (see [7]). Furthermore, one must keep in mind that the interval of spatial scale over which each fractal dimension was calculated has been kept identical from one image to another. These restrictions of the technique and the shape of the distribution obtained encourage us to consider the initial atomization process as a fractal process. Furthermore, the result presented in Fig. 5 shows the relevance of working with an average fractal dimension that corresponds to the most often encountered value. Similar results were obtained at other injection pressures and for the other liquids.

As mentioned above, working with local average fractal dimensions is physically representative. The determination of average fractal dimension can be achieved either by calculating the mean value of the distribution as the one shown in Fig. 5 or by plotting a single Richardson-Mandelbrot plot where the count shown on the ordinate axis is averaged on the image series. Both approaches are tested. Examples of local slope graphs obtained from the average Richardson-Mandelbrot plots are presented in Fig. 6.

The average local slope graphs shown in Fig. 6 re-enforce the idea that the liquid-gas interface is a fractal contour near the nozzle. In comparison with what was observed in Fig. 4 for one image only, the constant portion of local slope is more pronounced. Furthermore, Fig. 6 reports a clear influence of the downstream distance on the mean fractal dimension and the corresponding spatial scale range. As noted above, the textural fractal dimension increases with the downstream position as well as the spatial scale at which the local slope increases. This last behavior is a measure of the spatial expansion of the liquid jet in the (O, x, z) plane. Another interesting result to be mentioned here is that the mean fractal dimension obtained from the distribution (Fig. 5) is very near the fractal dimension calculated from the local slope graph of the average mean Richardson-Mandelbrot plot (Fig. 6). The difference between these two values does not exceed 1%. This value can be considered as the accuracy of the fractal dimension measurement.

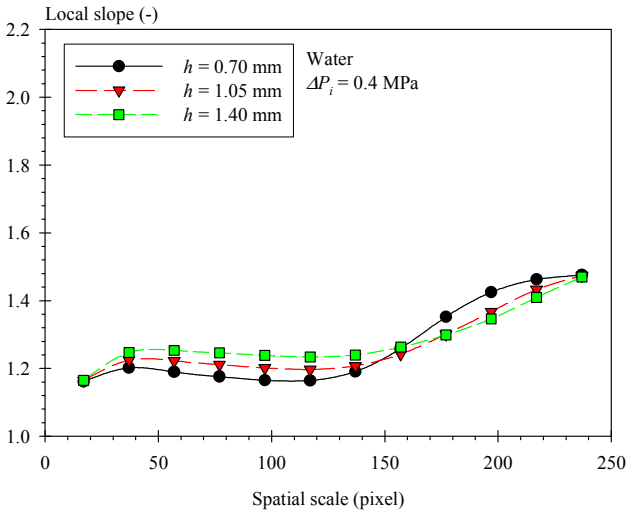

Figure 6: Local slope graphs obtained from the average Richardson-Mandelbrot plot (150 images, Water, ΔP_i = 0.4 MPa. Influence of the position from the nozzle.)

The mean textural fractal dimension of the liquid flow near the nozzle exit is determined for each liquid and for several injection pressures using the average Richardson-Mandelbrot plot. This is conducted for two positions of the analyzing window, namely, 0.7 mm and 1.05 mm. The results are presented in Fig. 7 where the textural fractal dimension is shown as a function of the Reynolds number of the issuing liquid flow (based on the discharge orifice diameter and the issuing mean velocity). Several important behavior must be noted. First, Fig. 7 reports a clear relationship between the textural fractal dimension and the Reynolds number of the issuing liquid flow, showing the relevance of the choice of this parameter. Globally speaking, it appears that the textural fractal dimension increases with the Reynolds number. For Reynolds numbers greater than 4000, the fractal dimension reports a non negligible scatter. For these points, it must be said that the interface is perturbed by very fine structures of the order of the spatial resolution of the image. Thus, the contour detection is less accurate and we believe that this affects the resulting fractal dimension. However, the dependence between the fractal dimension and the Reynolds number illustrates the impact of turbulence on the liquid gas interface as soon as the flow issues from the nozzle and that an increase of turbulence favors a greater

tortuosity of the interface and therefore a greater interface area production. Second, we can note that, for a given position of the analyzing window, the evolution of the textural fractal dimension versus the Reynolds number is independent of the injection pressure and of the liquid physical properties: the results obtained for all working conditions organize in a single behavior. Finally, it can be seen that the textural fractal dimension increases with the downstream position. This behavior, that was reported by previous investigations [4, 5], illustrates the growing of the perturbations initially induced by the turbulence.

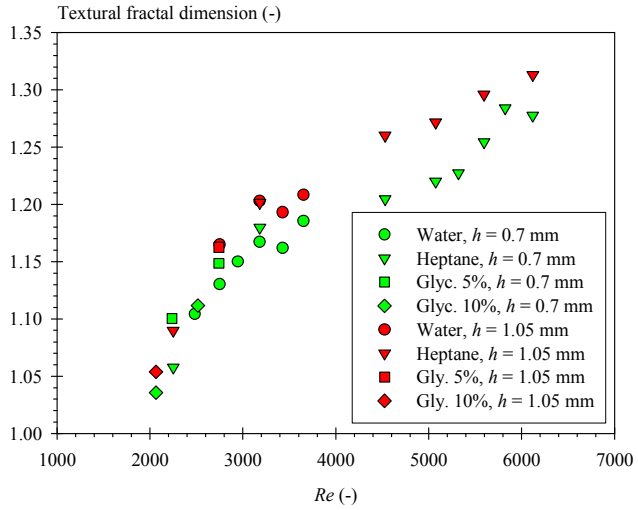

Figure 7: Textural fractal dimension of the liquid flow at primary atomization initial stage (near the nozzle) as a function of the Reynolds number. Influence of the position of the analyzing window (All fluids, all injection pressures)

The analysis conducted on the initial textural fractal dimension is repeated for the structural fractal dimension characterizing the ligament network of the final primary atomization step. In order to embrace all the ligament network, the height of the analyzing window is increased and taken equal to 512 pixels. Furthermore, for each image, the analyzing window is positioned such that the farthest contour pixel from the nozzle coincides with the bottom of the analyzing window. This arrangement is shown on the contour presented in Fig. 4 (dot-dash box).

As for the analysis of the initial textural fractal dimension, the first task consists in analyzing each image independently in order to produce the probability distribution of the structural fractal dimension of the ligament network. To achieve this and considering the results presented in Fig. 4, the structural fractal dimension is determined by calculating the slope of the individual Richardson-Mandelbrot plot for a range of spatial scales fixed to [111 pixels; 201 pixels].

The structural fractal dimension distribution obtained with water and an injection pressure of 0.4 MPa is shown in Fig. 8. As for the textural fractal dimension analyzed in Fig. 5, this distribution shows a bell shape with a clear maximum. The width of the distribution is however greater than the one obtained for the textural fractal dimension at the beginning of the atomization process. Here again, we have to keep in mind that the determination of the fractal dimension with the EDM method on a single image might be slightly inaccurate as observed in [7] and the use of a constant spatial scale range from one image to another to determine the fractal dimension might be also a source of inaccuracy. The production of the structural fractal dimension distribution suffers from another drawback. Contrary to the upper part of the liquid flow which is very similar from one image to another, the ligament network at the bottom of the continuous liquid flow might be partially atomized or totally detached from the continuous liquid flow. An example of a partially atomized ligament network is shown in Fig. 9. For this image, the structural fractal dimension of the lower part on the image is equal to 1.3, which belongs to the lower range of the distribution shown in Fig. 8. In contrary, when the ligament network is complete and still attached to the continuous liquid flow, the structural fractal dimension is of the order of 1.6 (see Fig. 4). Thus, the parts of the liquid flow analyzed for the production of Fig. 8 are not necessarily equivalent as far as the atomization process is concerned and the effect of this is an increase of the width of the distribution. From these considerations it can be concluded that the width of the distribution of the structural fractal dimension of the ligament network shown in Fig. 8 is overestimated and that the mean value given by this distribution is underestimated. However, the shape of the distribution encourages us to consider that the use of a fractal analysis is relevant to characterize the final stage of the atomization process.

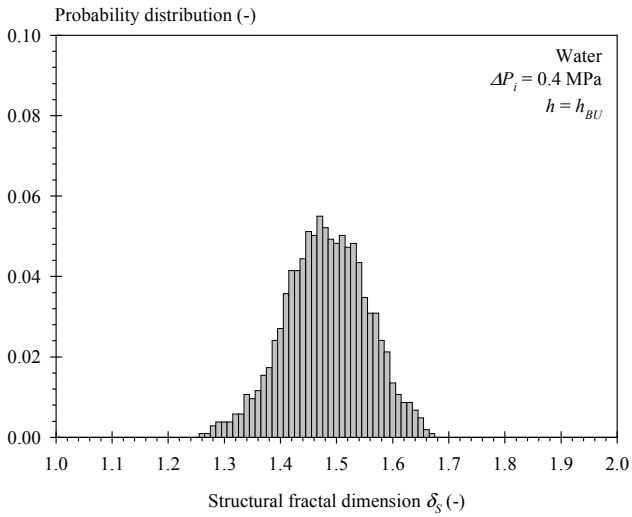

Figure 8: Probability distribution of the structural fractal dimension of the ligament network in the final stage of the atomization process (Water, ΔP_i = 0.4 MPa)

The shape of the distribution shown in Fig. 8 also indicates the relevance of defining a mean structural fractal dimension of the final stage of the liquid atomization process. As for the textural fractal dimension, the mean structural fractal dimension can be determined either by the probability distribution or by plotting the local slope graph of the average Richardson-Mandelbrot plot. For the experimental conditions corresponding to the situation shown in Fig. 8, the local slope graph of the average

Richardson-Mandelbrot plot is presented in Fig. 10. This figure shows that the lower part of the continuous liquid flow is clearly fractal over the large spatial scales investigated in the present work. Furthermore, it can be noticed that the fractal dimension reported by Fig. 10 ($\delta_s = 1.49$) and given by the constant local slope is very near the mean value obtained from Fig. 8, i.e., $\delta_s = 1.48$. Once again it is found that the two procedures to determine a mean fractal dimension agree to return the same value. In the following, the structural fractal dimensions shown are determined from the analysis of local slope graphs.

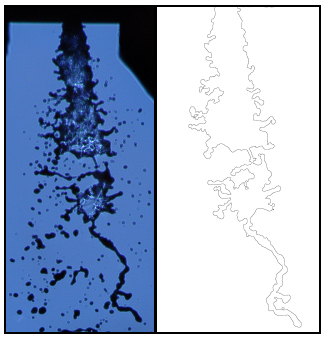

Figure 9: Partially atomized ligament network (Water, $\Delta P_i = 0.4$ MPa, $\delta_s = 1.3$)

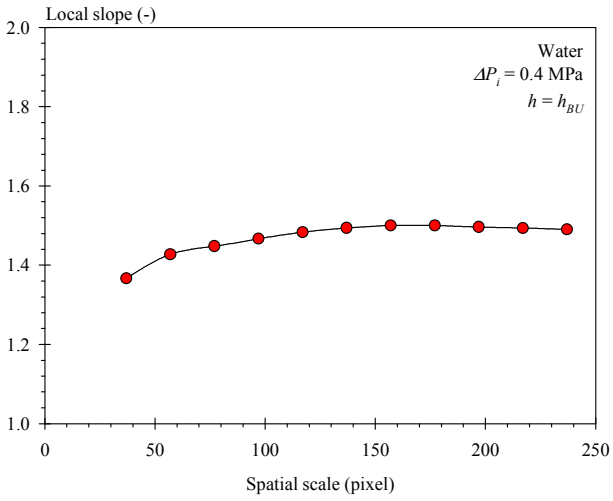

Figure 10: Local slope graph of the average Richardson-Mandelbrot plot. Bottom part of the liquid flow (Water, $\Delta P_i = 0.4$ MPa)

The structural fractal dimension of the bottom part of the continuous liquid flow is determined for all fluids and all injection pressures. The results are presented in Fig. 11 where the structural fractal dimension is presented versus the liquid Weber number calculated with the discharge orifice diameter, the average liquid velocity and the density and surface tension of the liquid.

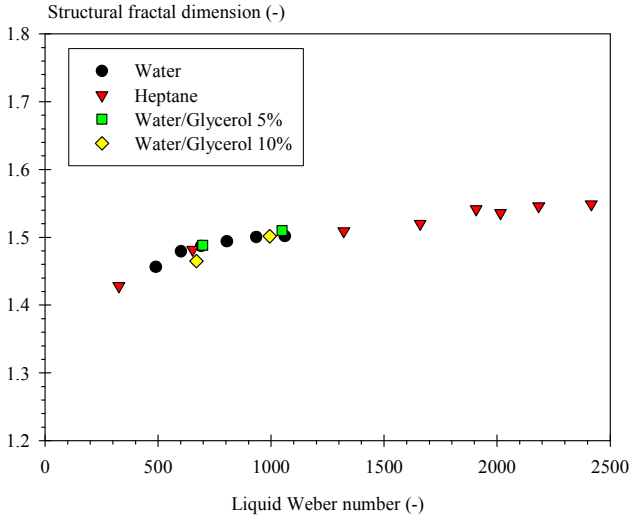

Figure 11: Evolution of the structural fractal dimension of the ligament network as a function of the liquid Weber number (All fluids, all injection pressures)

Figure 11 reports a single behavior regardless the injection pressure and the liquid: the structural fractal dimension slightly increases with the liquid Weber number and reaches an asymptotic value of the order of 1.52 as the liquid Weber number increases. This organization of the results with the liquid Weber number instead of the gaseous Weber number, is due to the fact that the aerodynamic forces have no effect on the atomization process. Furthermore, this result confirms that the evolution of the shape of the continuous liquid flow is mainly controlled by surface tension forces. Another important result shown in Fig. 11 is the existence of an asymptotic value of the structural fractal dimension of the lower part of the continuous liquid flow. This finding suggests that, for atomization processes controlled by surface tension, the production of interface for a given mass of liquid can not exceed a certain limit. The universality of this limit has to be proved. This limit is reached for liquid Weber number of the order 1500 as shown in Fig. 11. It can be also expressed in term of textural fractal dimension of the liquid flow near the nozzle exit.

Figure 12 displays the relationship between the textural fractal dimension of the upper part of the continuous liquid flow versus the structural fractal dimension of the lower part of the flow. A clear dependence between these two fractal dimensions appears in this figure but it seems that this dependence is a function of the physical properties of the liquid. An increase of the textural fractal dimension induces an increase of the structural dimension. However, for textural fractal dimensions greater than 1.20, all the structural fractal dimensions converge toward the limit seen in Fig. 11. This behavior indicates that although an increase of turbulence continuously increases the liquid gas interface area per unit volume near the nozzle, it has a limited effect on the interface area creation rate of the liquid structures from which most of the liquid volume is atomized.

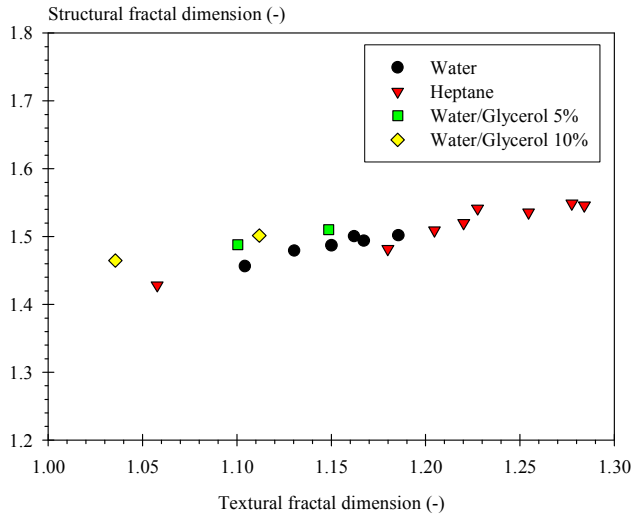

Figure 12: Relationship between the textural fractal dimension of the flow near the nozzle and the structural fractal dimension of the bottom part of the continuous liquid flow. (All fluids, all injection pressures)

4. CONCLUSIONS

The first important conclusion that can be drawn from this study is that atomizing liquid flows are fractal objects. Therefore, the use of fractal analysis to characterize the shape of an atomizing liquid flow is a relevant approach that can bring interesting results. Indeed, the dimension of a fractal object is a measure of its tortuosity. It informs on the surface area of the object according to its volume or on the perimeter of the object as a function of its surface area when working in 2D. During atomization processes, a given amount of liquid is deformed and sees an increase of its interface area until break-up occurs. A fractal analysis conducted on atomizing liquid flow is a measure of this deformation.

The fractal analysis conducted in the present work on liquid flows produced by a simplified compound injector used at low injection pressures shows first that the increase of the interface area near the nozzle exit is textural, i.e., it mainly affects the interface tortuosity without significantly modifying the whole shape of the flow. This deformation of the interface is directly controlled by the level of turbulence of the issuing liquid flow since a relationship between the textural fractal dimension and the Reynolds number of the flow has been found here independent of the nature of the liquid and of the injection pressure.

Second, it has been found that the increase of interface area in the latest stage of the atomization process is due to a modification of the whole shape of the flow and is therefore associated to a structural fractal dimension. This fractal dimension has been found related to the liquid Weber number of the flow regardless the liquid and the injection pressure. This behavior is due to the fact that, in the situations examined in this study, both deformation and break-up of the liquid flow are controlled by the surface tension forces. Furthermore, a limit value of the structural fractal dimension has been found. The limit value suggests that in atomization processes controlled by surface tension the creation of interface area per unit volume can not exceed a certain value.

5. NOMENCLATURE

C_D	Discharge coefficient [-]
h	Distance from the nozzle to the middle line of the analyzing window [mm]
h_{BU}	Farthest possible position of the analyzing window [mm]
L_{BU}	Break-up length [mm]
Q_v	Volume flow rate [m^3/s]
Re	Reynolds number of the issuing liquid flow [-]
S	Section of the nozzle discharge orifice [μm^2]
We_L	Liquid Weber number [-]
δ_S	Structural fractal dimension [-]
δ_T	Textural fractal dimension [-]
ΔP_i	Injection pressure [Pa]
μ	Liquid dynamic viscosity [kg/ms]
ρ_L	Liquid density [kg/m^3]
σ	Surface tension [N/m]

6. REFERENCES

1. Chigier, N., The Future of Atomization and Sprays, Proc. 20th Annual Conference on Liquid Atomization and Sprays Systems – Europe, Orléans, France, 2005
2. Kaye, B.H., A Random Walk Through Fractal Dimensions, VCH, New-York, 1989
3. Smith, T.G., Lange, G.D. and Marks, W.B., Fractal Methods and Results in Cellular Morphology – Dimensions, Lacunarity and Multifractals,Vol. 69, pp. 123-136, 1996
4. Shavit, U. and Chigier, N., Fractal Dimensions of Liquid Jet Interface Under Break-up. Atom. Sprays, Vol. 5, p. 525-543, 1995
5. Dumouchel, C., Cousin, J. and Triballier, K., Experimental Analysis of Liquid-Gas Interface at Low-Weber-Number: Interface Length and Fractal Dimension, Exp. Fluids, Vol. 39, p. 651-666, 2005
6. Dumouchel, C., Cousin, J. and Triballier, K., On the Role of the Liquid Flow Characteristics on Low-Weber-Number Atomization Processes. Exp. Fluids, Vol. 38, p. 637-647, 2005
7. Grout, S., Cousin, J. and Dumouchel, C., Fractal Analysis of Liquid Atomization Processes. Part 1: Methodology, Proc. of 10th International Conferencce of Liquid Atomization and Spray Systems, Paper ID ICLASS06-050, Kyoto, Japan, 2006
8. Sterling, A.M. and Sleicher, C.A., The Instability of Capillary Jets, JFM, Vol. 68, p. 477-495, 1975
9. Foroutan-pour, K., Dutilleul, P. and Smith, D.L., Advances in the Implementation of the Box-Counting Method of Fractal Dimension Estimation. Applied Math. And Comp., Vol. 105, p. 195-210, 1999
10. Panico, J. and Sterling, P., Retinal Neurons and Vessels Are Not Fractal But Space-Filling, The Journal of Comparative Neurology, Vol. 361, pp. 479-490, 1995